Influence of Jahn−Teller Coupling on the Magnetic Properties of Transition Metal Complexes with Orbital Triplet Ground Terms: Magnetization and Electronic Raman Studies of the Titanium(III) Hexa-Aqua Cation

P. L. W. Tregenna-Piggott* and Hans-Ueli Güdel

Department of Chemistry and Biochemistry, University of Bern, Freiestrasse 3, CH-3000, Bern 9, Switzerland

Received March 13, 2001

Magnetization and electronic Raman data are presented for salts of the type $Cs[Ga:Ti](SO_4)_2 \cdot 12H_2O$, which enable a very precise definition of the electronic structure of the $[Ti(OH_2)_6]^{3+}$ cation. The magnetization data exhibit a spectacular deviation from Brillouin behavior, with the magnetic moment highly dependent on the strength of the applied field at a given ratio of B/T. This arises from unprecedented higher-order contributions to the magnetization, and these measurements afford the determination of the ground-state Zeeman coefficients to third-order. The anomalous magnetic behavior is a manifestation of Jahn−Teller coupling, giving rise to low-lying vibronic states, which mix into the ground state through the magnetic field. Electronic Raman measurements of the 1%-titanium(III)-doped sample identify the first vibronic excitation at ~ 18 cm^{-1}, which betokens a substantial quenching of spin−orbit coupling by the vibronic interaction. The ground-state Zeeman coefficients are strongly dependent on the concentration of titanium(III) in the crystals, and this can be modeled as a function of one parameter, representing the degree of strain induced by the cooperative Jahn−Teller effect. This study clearly demonstrates the importance that the Jahn−Teller effect can have in governing the magnetic properties of transition metal complexes with orbital triplet ground terms.

1. Introduction

The measurement of the magnetic response of a given material is one of the oldest physical methods with which to probe its electronic and molecular structure. The way to calculate the paramagnetic susceptibility was first set out by J. H. Van Vleck in 1932[1] and applied to explain magnetic data from a number of inorganic salts.[2] In light of the Jahn−Teller theorem formulated soon afterwards,[3] it was inferred that in instances where the crystal field leaves an orbitally degenerate ground state, both the electronic and vibrational coordinates of the system should be considered when a satisfactory explanation of its magnetic properties is sought.[4] The proof of the theorem rests on group theory, which says nothing about the strength of coupling between the electronic and vibrational states. Hence the assessment of its implication, as expounded by J. S. Griffith, "...from a purely logical point of view we mean that the effect occurs, unless it does not occur, and have therefore said nothing useful...;"[5] and in a similar vein from J. H. Van Vleck, "It is a great merit of the Jahn−Teller effect that it disappears when not needed".[2]

Ever since the first unequivocal observation of the Jahn−Teller effect in the EPR spectrum of copper-doped zinc fluorosilicate,[6] many studies on this phenomenon have remained focused on octahedrally coordinated copper(II) complexes, where the orbital degeneracy occurs in the strongly σ-antibonding e_g orbital set.[7] In comparison, the effect of Jahn−Teller coupling on the electronic properties of transition metal complexes, where the orbital degeneracy occurs in the t_{2g} orbital set, has all too often been placed into the "not needed" category, on the basis that the t_{2g} orbitals are either nonbonding or weakly π-antibonding. Notwithstanding that the manifestation of Jahn−Teller coupling in complexes with orbital triplet ground terms has played a pivotal role, in understanding the subtleties of the phenomenon,[8] the influence on the magnetic properties of these systems has not been fully appreciated by magnetochemists. Although it is certainly true that copper(II) complexes usually provide archetypal examples of vibronically induced structural instability, the effect of Jahn−Teller coupling on their magnetic properties is relatively minor, when compared to that expected for complexes with orbital triplet ground terms subject to fairly modest Jahn−Teller coupling. This is because the deviation of the magnetic properties of transition metal complexes from spin-only behavior depends on the extent to which orbital angular momentum is quenched by the crystal field; orbital angular momentum acts to first-order in triplet ground terms but only

* Corresponding author. E-mail: tregenna@iac.unibe.ch. Phone: 00-41-31-631-4317. Fax: 00-41-31-631-4322.

(1) Van Vleck, J. H. *Electric and Magnetic Susceptibilities*; Oxford University Press: New York, 1932.
(2) Van Vleck, J. H. *J. Chem. Phys.* **1939**, *7*, 61−71.
(3) Jahn, H. A.; Teller, E. *Phys. Rev.* **1936**, *49*, 874; *Proc. R. Soc. London, Ser. A* **1937**, *161*, 220.
(4) Van Vleck, J. H. *J. Chem. Phys.* **1939**, *7*, 72−84.
(5) Griffith, J. S. *The Theory of Transition-Metal Ions*; Cambridge University Press: New York, 1961; p 209.
(6) Bleaney, B.; Ingram, D. J. E. *Proc. Phys. Soc., London* **1950**, *63*, 408. Bleaney, B.; Bowers, K. D. *Proc. Phys. Soc., London* **1952**, *65*, 667.
(7) Hitchman, M. A.; Maaskant, W.; Van der Plas, J.; Simmons, C. J.; Stratemeier, H. *J. Am. Chem. Soc.* **1999**, *121*, 1488−1501 and references therein.
(8) Sturge, M. D. *Solid State Phys.* **1967**, *20*, 91. Ham, F. S. Jahn−Teller Effects in Electron Paramagnetic Resonance Spectra. In *Electron Paramagnetic Resonance*; Geshwind, S., Ed.; Plenum Press: New York, 1972. Englman, R. *The Jahn−Teller Effect in Molecules and Crystals*; Wiley: London, 1972. Bersuker, I. B. *The Jahn−Teller Effect and Vibronic Interactions in Modern Chemistry*; Plenum Press: New York, 1984.

10.1021/ic010277f CCC: $20.00
Published on Web 09/18/2001

to second-order in doublet ground terms (cubic symmetry); and the effects of both the orbital Zeeman and spin−orbit coupling operators are redistributed by the Jahn−Teller interaction across the vibronic spectrum. To illustrate this phenomenon, magnetic data are presented and modeled from a chemical system no less intriguing than the celebrated molecular magnet "Mn_{12}"[9] and whose electronic structure has proved more elusive than that of ascidian blood cells:[10] a monomeric, homoleptic d^1 complex, the $[Ti(OH_2)_6]^{3+}$ cation.

The magnetic properties of $Cs(OH_2)_6Ti(OH_6)_6(SO_4)_2$, CsTiSH, and related systems have baffled magnetochemists for more than 60 years.[2,11−22] The high site symmetry of the $[Ti(OH_2)_6]^{3+}$ cation (S_6) and large Ti(III)−Ti(III) separation[23,24] (ca. 8.7 Å) would suggest this to be an ideal host in which to study the magnetic behavior of a $3d^1$ complex. However, only recently, due to the combined efforts of a number of groups, has certain progress towards defining the electronic structure of the $[Ti(OH_2)_6]^{3+}$ cation in this ostensibly simple system been made.[25−31] The complexity arises from a delicate balance between spin−orbit and Jahn−Teller coupling, as revealed from a detailed analysis of the variation of the effective magnetic moment with temperature for CsTiSH and titanium(III) doped into the isostructural $Cs(OH_2)_6Ga(OH_6)_6(SO_4)_2$ salt (CsGaSH, Cs[Ga:Ti]SH).[29] The study was confined to the temperature range of 15−295 K, where the $[Ti(OH_2)_6]^{3+}$ cation is axially symmetric. As the temperature is lowered below ca. 12 K, CsTiSH undergoes a cubic-to-orthorhombic phase transition, driven by the cooperative Jahn−Teller effect, which gives rise to a lowering of the site symmetry of the $[Ti(OH_2)_6]^{3+}$ cation from S_6 to C_i.[28]

The present work provides a detailed examination of the magnetic properties of Cs[Ga:Ti]SH in the temperature range of 1.7−12 K and the magnetic field range of 1.0−5.5 Tesla. We set out to show the anomalous magnetic behavior arising from the Jahn−Teller interaction and how this phenomenon is strongly attenuated by low-symmetry distortions. The latter objective is realized chemically by examining salts with varying concentrations of titanium(III) (1, 13, 51, and 100% of the total tervalent cation concentration), thereby tuning the degree of cooperative interactions between the Jahn−Teller centers. Preliminary magnetization data for the 1%-titanium(III)-doped sample have already been presented in a previous communication.[30]

The magnetic properties of the samples are revealed by obtaining an extensive data set of the magnetic moment as a function of both field and temperature. This affords a two-dimensional representation of the magnetic properties of the system from which the ground-state Zeeman coefficients are precisely determined to third-order. The magnetic data are complemented by Raman measurements, which provide a direct measure of the energy of the first excited state. The second-order contribution to the magnetization is, to our knowledge, the largest ever reported for a spin-half system and is shown to arise as a consequence of Jahn−Teller coupling. The ground-state Zeeman coefficients vary dramatically with the titanium(III) concentration, and this can be modeled by varying just one parameter, representing the deviation of $[Ti(OH_2)_6]^{3+}$ from trigonal symmetry.

2. Experimental Section

CsTiSH and CsGaSH were prepared following methods described in the literature (Ga[24] and Ti[32]). Polycrystalline material of Cs[Ga:Ti]SH was prepared by cocrystallization of CsGaSH and CsTiSH in H_2SO_4 (1 M), and large single crystals grown by slow deposition of material on a seed, suspended in a saturated solution of the mother liquor. Four single crystals were prepared with differing concentrations of titanium(III); each crystal was subjected to Raman and magnetization measurements. Scattering experiments were conducted of the type $X'(\alpha\beta)Y'$, where X' and Y' are related to the crystallographic X and Y directions by a rotation of $\pi/4$ about $Z = [100]$ and $\alpha\beta$ is the component of the polarizability tensor under examination. In these experiments, $a_g + e_g$ modes are active when $\alpha\beta = ZZ$, e_g when $\alpha\beta = Y'X'$, and f_g when $\alpha\beta = ZX'$ or $Y'Z$. Faces of the types [110] corresponding to the incident and exit directions of the laser and [$\bar{1}$10] corresponding to the collection direction of the scattered radiation were hewn using a diamond saw and polished on a surface onto which 1 μm Al_2O_3 was dispersed. Epoxy glue (Araldite Rapid) was used to attach the crystal to a three-circle goniometer head, which was placed in the sample space of either an Oxford Instruments MD4 bath cryostat (spectra obtained for Cs[Ga:Ti]SH samples, temperature estimated using a RhFe resistor at the heat exchanger) or an Oxford Instruments 20 mm bath cryostat (spectra recorded for a CsTiSH sample, temperature estimated from readings taken from a Cernox sensor positioned close to the sample). Raman spectra were collected using a Spex 1402 double monochromator fitted with 1800 grooves/mm holographic gratings and a RCA C31034 photomultiplier tube. The samples were excited with radiation provided by either a Spectra Physics 2060-10 SA Ar laser or a Coherent CR 500K Kr laser. The radiation was focused onto the sample using a Melloes Griot precision-optimized achromat in conjunction with an aplanar meniscus lens (combined focal length ≈ 50 mm) and collected using a Canon 50/1.2 camera lens.

The magnetization measurements were performed on SQUID magnetometers at the University of Monash, University of Zürich, and University of Bern. The data obtained from the three instruments were consistent. The crystals were hewn down to a size such that they were

(9) Mirebeau, I.; Hennion, M.; Casalta, H.; Andres, H.-P.; Güdel, H.-U.; Irodova, A. V.; Caneschi, A. *Phys. Rev. Lett.* **1999**, *83*, 628.
(10) Metal Ions in Biological Systems. In *Vanadium and its Role in Life*; Sigel, H., Sigel, A., Eds.; Marcel Dekker: New York, 1995; Vol. 31.
(11) Bijl, D. *Proc. Phys. Soc., London* **1950**, *63*, 407.
(12) Benzie, R. J.; Cooke, A. H. *Proc. R. Soc. London, Ser. A* **1951**, *209*, 269−278.
(13) Bleaney, B.; Bogle, G. S.; Cooke, A. H.; Duffus, R. J.; O'Brien, M. C. M.; Stevens, K. W. H. *Proc. Phys. Soc., London* **1955**, *68*, 57.
(14) Bose, A.; Chakravarty, A. S.; Chatterjee, R. *Proc. R. Soc. London, Ser. A* **1960**, *255*, 145. Bose, A.; Chakravarty, A. S.; Chatterjee, R. *Indian J. Phys.* **1959**, *33*, 325. Dutta-Roy, S. K.; Chakravarty, A. S.; Bose, A. *Indian J. Phys.* **1959**, *33*, 483.
(15) Figgis, B. N.; Lewis, J.; Mabbs, F. E. *J. Chem. Soc.* **1963**, 2473.
(16) Gladney, H. M.; Swalen, J. D. *J. Chem. Phys.* **1965**, *42*, 1999.
(17) Mackinnon, J. A.; Bickerton, J. L. *Can. J. Phys.* **1970**, *48*, 814.
(18) Manoogian, A. *Can. J. Phys.* **1970**, *48*, 2577.
(19) Dionne, G. F. *Can. J. Phys.* **1972**, *50*, 2232.
(20) Harrowfield, B. V. *Phys. Abstr.* **1972**, *75*, 594, No. 10288.
(21) Shing, Y. H.; Walsh, D. *Phys. Rev. Lett.* **1974**, *33*, 1067. Jesion, A.; Shing, Y. H.; Walsh, D. In *Proceedings of the Eighteenth Ampere Congress*; Nottingham, England, Sept 9−14, 1974; Allen, P. S., Andrew, E. R., Bates, C. A., Eds.; University of Nottingham Press: Nottingham, England, 1975; p 561. Jesion, A.; Shing, Y. H.; Walsh, D. *Phys. Rev. Lett.* **1975**, *35*, 51.
(22) Tachikawa, H.; Murakami, A. *J. Phys. Chem.* **1995**, *99*, 11046−11050.
(23) Sygusch, J. *Acta Crystallogr., Sect. B* **1974**, *30*, 662−665.
(24) Beattie, J. K.; Best, S. P.; Skelton, B. W.; White, A. H. *J. Chem. Soc., Dalton Trans.* **1981**, 2105−2111.
(25) Daul, C.; Goursot, A. *Inorg. Chem.* **1985**, *24*, 3554−3558.
(26) Best, S. P.; Forsyth, J. B. *J. Chem. Soc., Dalton Trans.* **1991**, 1721−1725.
(27) Dubicki, L.; Riley, M. J. *J. Chem. Phys.* **1997**, *106*, 1669.
(28) Tregenna-Piggott, P. L. W.; Best, S. P.; O'Brien, M. C. M.; Knight, K. S.; Forsyth, J. B.; Pilbrow, J. R. *J. Am. Chem. Soc.* **1997**, *119*, 3324−3332.
(29) Tregenna-Piggott, P. L. W.; O'Brien, M. C. M.; Pilbrow, J. R.; Güdel, H.-U.; Best, S. P.; Noble, C. *J. Chem. Phys.* **1997**, *107*, 8275.
(30) Tregenna-Piggott, P. L. W.; O'Brien, M. C. M.; Weihe, H.; Güdel, H. U. *J. Chem. Phys.* **1998**, *109*, 2967.
(31) Tregenna-Piggott, P. L. W.; Noble, C. J.; Pilbrow, J. R. *J. Chem. Phys.* **2000**, *113*, 3289.
(32) Best, S. P.; Armstrong, R. S.; Beattie, J. K. *Inorg. Chem.* **1980**, *19*, 1958.

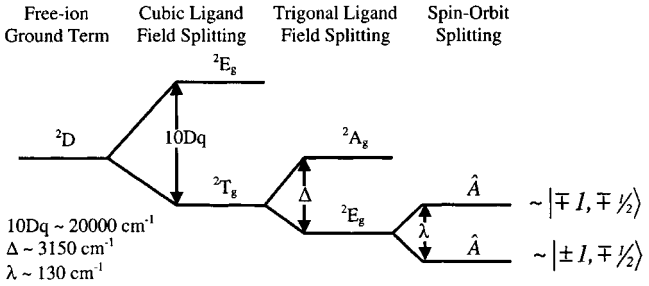

Figure 1. Schematic diagram showing the effects of the ligand field and spin−orbit splittings on the states of the ^{2}D free-ion term, whose wave functions are specified as $|m_l, m_s\rangle$. The sign and magnitude of the trigonal field, Δ, are taken from the work of Best.[26]

suitable for single-crystal Raman measurements and also fitted snugly into a SQUID measurement straw, thus dispensing with the need for a single-crystal sample holder. All magnetic measurements were performed with the [100] direction of the crystal aligned parallel with the external field. Data were collected as a function of temperature for fixed values of magnetic field. The length of the crystals was typically 5 mm along the [100] direction, thus deviating substantially from the idealized point dipole criteria that one must approach in order to obtain an accurate measure of the magnetic moment. As we shall show, the low-temperature, high-field magnetization data are very dependent on the titanium(III) concentration; however, the magnetic susceptibility of the $[Ti(OH_2)_6]^{3+}$ complex obtained in the temperature range of 15−290 K is independent of the titanium(III) concentration as we have shown previously.[29] The loss in signal due to the excessive length of the crystal was corrected for by comparison of the low-field, high-temperature data with that obtained from CsTiSH. Repeated measurements on different samples of CsTiSH of small dimensions using different instruments suggested that the CsTiSH data were both precise and accurate. The susceptibility data derived for CsTiSH[29] were plotted against data obtained at 2000 G, between 15 and 295 K, for each sample, and an excellent linear fit was obtained. From the gradient, intercept, and literature values for the diamagnetic susceptibilities of CsTiSH and CsGaSH, the concentration of titanium(III) in the sample as well as an effective mass could be derived. The effective mass assumes a uniform density and titanium(III) distribution on the macroscopic level and was typically 85% of the actual mass, this being a direct consequence of the large sample size. From knowledge of the concentration of titanium(III) in the sample and its effective mass, determined from the low-field, high-temperature region, the paramagnetic moment of the $[Ti(OH_2)_6]^{3+}$ complex could be calculated in the low-temperature, high-field range of interest. Magnetic data obtained within ca. 0.1 K of the lambda point of liquid helium were found to be inconsistent with the rest of the data set, for every sample and on every instrument, and hence were not included in the final analysis.

3. Theory

3.1. Vibronic Hamiltonian. The starting point for the vibronic calculations follows from the ligand-field calculations of Best, who rationalized the sign and magnitude of the trigonal field on the basis of careful neutron structure determinations of the cesium alums combined with AOM calculations.[26] The action of the ligand field and spin−orbit coupling on the states of the ^{2}D free-ion term is shown in Figure 1. Following the approach we employed in the analysis of the variation of the effective magnetic moment of CsTiSH between 15 and 295 K,[29] the electronic basis is confined to the ground trigonal ^2E_g term on account of the large trigonal and cubic fields.

The Hamiltonian describing the vibronic interaction between the ^2E_g (S_6) ground term and a spectrum of e_g phonons in the presence of a small low-symmetry crystal field may be written as

$$H = E_0\tau + \sum_i (1/2\mu_i)[P_{\theta_i}^2 + P_{\epsilon_i}^2 + \mu_i^2\omega_i^2(Q_{\theta_i}^2 + Q_{\epsilon_i}^2)]\tau + V_i[Q_{\theta_i}U_\theta + Q_{\epsilon_i}U_\epsilon] + e_\theta U_\theta + e_\epsilon U_\epsilon + \lambda L\cdot S + B\mu_B(kL + 2S) \quad (1)$$

where λ is the spin−orbit coupling parameter, k is the orbital reduction factor, and μ_B is the Bohr magneton. E_0 is the energy of the doubly degenerate electronic state resulting from the cubic and trigonal components of the crystal field, P_{θ_i} and P_{ϵ_i} are the momenta conjugate to Q_{θ_i} and Q_{ϵ_i}, μ_i is the effective mass of the ith phonon mode, and ω_i is its angular frequency. V_i is the linear Jahn−Teller coupling coefficient between the doublet electronic state and the ith phonon mode, and is related to the Jahn−Teller stabilization energy, E_{JT_i}, through the relation

$$E_{JT_i} = \frac{V_i^2}{2\mu_i\omega_i^2} \quad (2)$$

τ, U_θ, and U_ϵ are the Hermitian electronic operators transforming as A_g and the θ, ϵ components of the two-dimensional irreducible representation E_g, in the S_6 point group. It is convenient to work in the complex electronic basis, writing the electronic wave functions in terms of their respective m_l and m_s quantum numbers as $|-1, \pm 1/2\rangle$, $|1, \pm 1/2\rangle$, with the quantization axis along the direction of the trigonal field. In this basis, U_θ and U_ϵ take the form of the Pauli matrices:

$$U_\theta = \begin{pmatrix} 0 & 1 \\ 1 & 0 \end{pmatrix}; \quad U_\epsilon = \begin{pmatrix} 0 & -i \\ i & 0 \end{pmatrix} \quad (3)$$

The Hamiltonian (eq 1) is analogous to that employed to calculate the variation of the effective magnetic moment of CsTiSH between 15 and 295 K,[29] except that the terms $e_\theta U_\theta$ and $e_\epsilon U_\epsilon$, otherwise known as strain terms, are added to describe the effect of a low-symmetry crystal field. The Hamiltonian does not describe long-range interactions between the distortions of the $[Ti(OH_2)_6]^{3+}$ centers. For the purpose of this work, it is sufficient to recognize that such cooperative interactions give rise to a genuine lowering of symmetry of the $[Ti(OH_2)_6]^{3+}$ cations below a critical temperature.[33,34] Provided we confine our attention to linear Jahn−Teller coupling in the ^2E_g basis, strains of symmetries E_θ and E_ϵ have the same effect on the energies of the vibronic states. Therefore, for the purpose of our calculations, the two quantities in the Hamiltonian representing the low-symmetry crystal field may be reduced to one, e_θ, where $2e_\theta$ is equivalent to the one-electron splitting of the ^2E_g ground term. Each electronic basis function was then expanded in terms of the N_v levels of two two-dimensional harmonic oscillators. The eigenvalues and eigenvectors of the Hamiltonian (eq 1) were determined numerically using a Lanczos algorithm as described previously.[29]

Unless otherwise stated, the theoretical Zeeman coefficients and electronic Raman spectra were calculated with the same parameters used to model the high-temperature susceptibility data of CsTiSH ($k = 0.88$, $\lambda = 130$ cm^{-1}, $\hbar\omega_1 = 894$ cm^{-1}, $E_{JT1} = 90.1$ cm^{-1}, $\hbar\omega_2 = 53$ cm^{-1}, $E_{JT2} = 53$ cm^{-1}) with the

(33) Gehring, G. A.; Gehring, K. A. *Rep. Prog. Phys.* **1975**, *38*, 1−89.
(34) Kaplan, M. D.; Vekhter, B. G. *Cooperative Phenomena in Jahn−Teller Crystals*; Plenum Press: New York, 1995.

addition of low-symmetry strain represented by the parameter e_θ. Henceforth, these parameters shall be collectively known as the two-mode model. Adequate numerical convergence was obtained with N_v set to 10 for both modes, which required the diagonlization of a sparse matrix of dimension 17 424.

Zeeman coefficients (denoted by the symbol W) higher than second-order were evaluated by calculating the eigenvalues of the ground Kramers doublet as a function of field from 0 to 5.5 Tesla (the highest experimental field) and fitting the resulting relation to a power series in field. When Zeeman coefficients only up to second-order were required, it was sufficient to perform the calculation once with $B = 0$ Tesla and once with $B = 0.1$ Tesla and to include terms in the expansion to second-order only.

The zero-order electronic Raman cross section for a transition from state i to state f, in a $X'(Y'X')Y'$ polarization, was calculated according to

$$(E_0 - (E_f - E_i))^4 \exp\left(\frac{-E_i}{kT}\right)\langle\psi_i|\hat{\alpha}_{X'Y'}|\psi_f\rangle(\langle\psi_i|\hat{\alpha}_{X'Y'}|\psi_f\rangle)^* \quad (4)$$

where E_0 is the energy of the incident radiation and E_i and E_f the energies of the states i and f relative to E_0. ψ_i and ψ_f are the vibronic wave functions expressed as linear combinations of the original uncoupled functions. The matrix elements were evaluated by expanding the electronic Raman scattering tensor in terms of orbital angular momentum operators. For Raman experiments, which select the $\hat{\alpha}_{X'Y'}$ component of the polarizability tensor, only transitions of E_g activity are allowed. As our electronic basis is confined to the states of the ^2E_g ground term (eq 3), $\hat{\alpha}_{X'Y'}$ takes the form of $\hat{L}_+^2 + \hat{L}_-^2$. Thus, the electronic Raman operator links states that differ by two in the m_l quantum number ($1 \leftrightarrow -1$) with the spin and vibrational quantum numbers remaining unchanged. Raman transitions were folded with a Lorentzian band shape function with a constant width across the spectrum.

3.2. Magnetic Moment of the Ground Kramers Doublet. A general expression for the magnetic moment of a Kramers doublet may be formulated by expanding the energies of the two states as a power series in field, evaluating the differential $-dE/dB$, and applying Boltzmann statistics. The magnetic moment, in units of μ_B/ion, is then given by

$$M = \tanh(y)\sum_{i,\text{odd}}^{i\le n} -iW^{(i)}B^{i-1} + \sum_{i,\text{even}}^{i\le n} -iW^{(i)}B^{i-1} \quad (5)$$

where

$$y = \frac{\sum_{i,\text{odd}}^{i\le n} -\mu_B W^{(i)}B^i}{k_B T}$$

where $W^{(i)}$ is the Zeeman coefficient of ith order. If the expansion is terminated at $n = 1$, eq 5 reduces to the well-known Brillouin function

$$M = W^{(1)}\tanh(W^{(1)}\mu_B B/k_B T) \quad \mu_B/\text{ion} \quad (6)$$

When $E_{JT} = 0$, expressions for the Zeeman coefficients may be easily obtained using standard methods of perturbation theory. In the absence of strain, Zeeman coefficients to third-order are given by

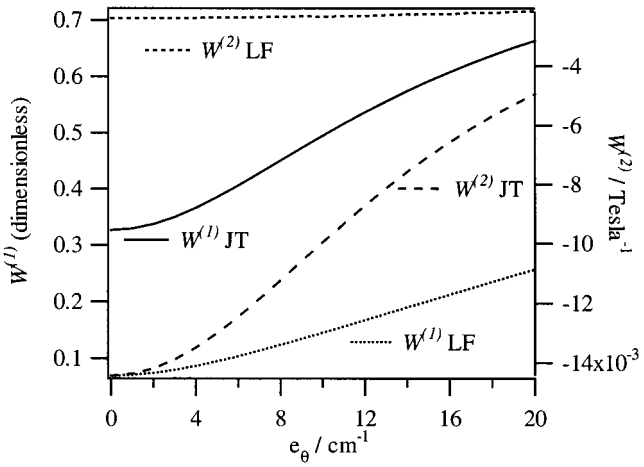

Figure 2. Theoretical values of $W^{(1)}$ and $W^{(2)}$ for $\theta = 54.74°$ as a function of the strain parameter, e_θ. Plots denoted by LF (ligand field) were calculated assuming no vibronic coupling; plots denoted by JT (Jahn−Teller) were calculated with $\hbar\omega_1 = 894$ cm^{-1}, $E_{JT1} = 90.1$ cm^{-1}, $\hbar\omega_2 = 53$ cm^{-1}, $E_{JT2} = 53$ cm^{-1} (two-mode model).

$$W_\theta^{(1)} = \pm(1 - k)\cos\theta \qquad \text{(dimensionless)} \quad (7)$$

$$W_\theta^{(2)} = -\frac{\sin^2\theta\,\mu_B}{\lambda} \qquad (\text{Tesla}^{-1}) \quad (8)$$

$$W_\theta^{(3)} = \mp\frac{W^{(1)}(W^{(2)})^2}{\sin^2\theta} \qquad (\text{Tesla}^{-2}) \quad (9)$$

where θ is the angle between the magnetic field direction and the principal S_6 axis of the molecule. For a finite value of e_θ, in the limit where $\lambda \gg e_\theta \gg B\mu_B$, $W^{(1)}$ and $W^{(2)}$ become

$$W_\theta^{(1)} \approx \left(\left(1 - k\left(\frac{2\lambda^2}{\lambda^2 + e_\theta^2} - 1\right)\right)^2\cos\theta^2 + \left(\frac{4e_\theta\lambda}{\lambda^2 + e_\theta^2}\right)^2\sin\theta^2\right)^{1/2}$$
(dimensionless) (10)

$$W_\theta^{(2)} \approx -\frac{(4e_\theta^2k^2\cos^2\theta + (\lambda^2 - 2e_\theta^2)\sin^2\theta)\mu_B}{\lambda^3 + 4e_\theta^2\lambda} \qquad (\text{Tesla}^{-1}) \quad (11)$$

Figure 2 shows plots of $W^{(1)}$ and $W^{(2)}$ as a function of e_θ, with $\lambda = 130$ cm^{-1}, $k = 0.88$, and $\theta = 54.74°$ (LF plots). Although the relations were calculated numerically, the LF plots are well described by eqs 10 and 11. It is seen from these equations and Figure 2 that a small low-symmetry distortion gives rise to a sharp increase in $W^{(1)}$ (approximately first-order in e_θ), and a slight decrease in $W^{(2)}$ (approximately second-order in e_θ). The decrease in $W^{(2)}$ with increasing e_θ is due primarily to the reduction of the expectation value of the off-diagonal Zeeman operator on account of the changing basis. The lower the value of λ, the easier it is for the two states to mix through a low-symmetry distortion and the more rapidly $W^{(2)}$ will tend towards zero. When $\lambda = 0$ and $e_\theta \gg B\mu_B$, $W_\perp^{(1)} = 1$ and $W_\perp^{(2)} = 0$.

Superimposed on Figure 2 are plots of $W^{(1)}$ and $W^{(2)}$ as a function of e_θ, calculated using the Jahn−Teller two-mode model (JT plots). Comparison of plots LF and JT in Figure 2 shows that the increase in $W^{(1)}$ as a function of strain is greatly enhanced by the Jahn−Teller effect. For a detailed discussion

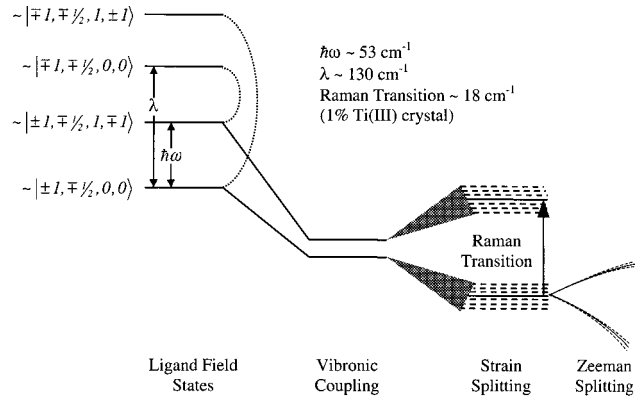

Figure 3. Schematic diagram showing the effects of the Jahn−Teller, strain, and Zeeman interactions on the states of the ^2E_g ground term. The diagram starts where Figure 1 finishes. The states are specified as $|m_l, m_s, N, M\rangle$, and the figure depicts the Jahn−Teller matrix elements between the ground and first vibrational excitations by means of curved broken lines.

of the dependence of the ground-state g values of this system ($g \equiv 2W^{(1)}$) on strain and Jahn−Teller coupling, refer to refs 27 and 31; the dependence of $W^{(2)}$ on E_{JT} and e_θ has not been addressed before and is of primary interest here. Coupling of the electronic states to the low-energy mode at 53 cm^{-1} is largely responsible for the dramatic increase in the magnitude of the ground-state value of $W^{(2)}$, and this can be illustrated using a simple perturbation model. In the limit where $\lambda \gg \hbar\omega \gg \sqrt{2E_{JT}\hbar\omega} \gg B\mu_B$, the energies and wave functions of the ground and first excited states (specified as, $|m_l, m_s, N, M\rangle$, where N and M are the principal quantum numbers of the 2-d harmonic oscillator) are

$$E_0 = -\frac{2E_{JT}\hbar\omega}{\lambda + \hbar\omega}$$

$$\psi_0 \approx |\pm 1, \mp 1/2, 0, 0\rangle - \frac{\sqrt{2E_{JT}\hbar\omega}}{\lambda + \hbar\omega}|\mp 1, \mp 1/2, 1, \pm 1\rangle \qquad (12)$$

$$E_1 = \hbar\omega - \frac{2E_{JT}\hbar\omega}{\lambda - \hbar\omega}$$

$$\psi_1 \approx |\pm 1, \mp 1/2, 1, \mp 1\rangle - \frac{\sqrt{2E_{JT}\hbar\omega}}{\lambda - \hbar\omega}|\mp 1, \mp 1/2, 0, 0\rangle \qquad (13)$$

As a result of the Jahn−Teller interaction, some of the electronic properties of the upper Kramers doublet are transferred to the first vibrational excitation and the energy gap relative to the ground state is diminished, as depicted in Figure 3. This is the basis for the effective quenching of the spin−orbit coupling interaction,[35] as seen in the ground state, which is manifested in an enhancement of $W^{(2)}$. From eqs 12 and 13, the contribution from the first excitation to the overall ground-state $W^{(2)}$ is

$$W^{(2)}_{0,1} \approx -\frac{2E_{JT}\sin^2\theta\mu_B}{\lambda^2 - 2\hbar\omega\lambda}(\lambda \gg \hbar\omega) \quad (\text{Tesla}^{-1}) \qquad (14)$$

Whereas the Jahn−Teller interaction mixes states that differ by one in the quantum numbers N and M, strain mixes states with the same vibrational quantum numbers. The two interactions compete, having contrary effects on the magnitude of $W^{(2)}$. It is seen from plot $W^{(2)}$ JT, displayed in Figure 2, that the enhancement of $W^{(2)}$ brought about by the Jahn−Teller interaction is strongly attenuated by low-symmetry strain. Compared to the LF plot, the decrease in $W^{(2)}$ is much sharper for a given value of e_θ as a consequence of the effective reduction of λ by the Jahn−Teller interaction. Therefore, a strong signature of the presence of significant Jahn−Teller coupling is an anomalously large value of $W^{(2)}$, which is expected to be strongly moderated by low-symmetry distortions.

(35) Ham, F. S. *Phys. Rev.* **1965**, *138*, 1727. Ham, F. S. *Phys. Rev.* **1968**, *166*, 307.

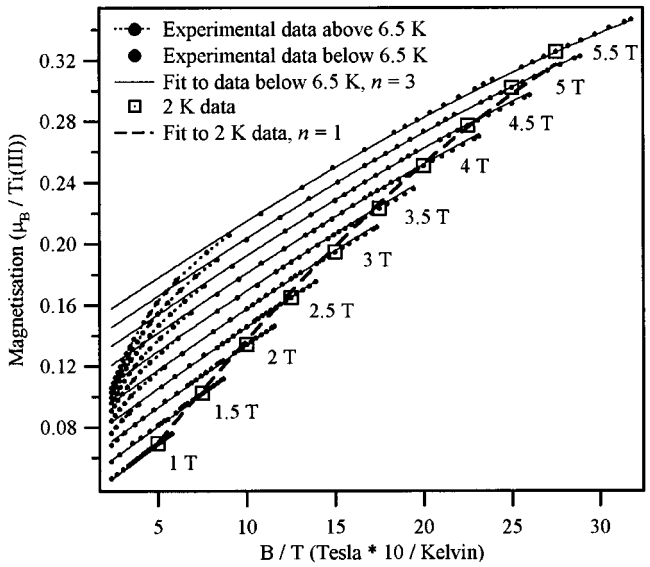

Figure 4. Magnetization vs B/T obtained from a single crystal of Cs[Ga:Ti]SH (ca. 0.4 g) where titanium(III) constitutes ca. 1% of the total tervalent cation concentration. The [100] direction of the crystal was aligned parallel with the external field. Experimental data are overlaid with two fits obtained using eq 5, with $n = 1$ and 3. The least-squares fit to the 2 K data with $n = 1$ yields $W^{(1)} = \pm 0.460(2)$. The least-squares fit to all of the data below 6.5 K with $n = 3$ yields $W^{(1)} = \pm 0.3572(4)$, $W^{(2)} = -0.01244(4)$ Tesla^{-1}, and $W^{(3)} = \mp 0.000326(5)$ Tesla^{-2}.

4. Results

4.1. Magnetization Data. Although the magnetic susceptibility of a cubic crystal is independent of orientation with respect to the external field, the magnetization at low temperatures and high fields is strongly orientation dependent when the magnetic anisotropy of the constituent ions is very large, as is the case here. All the magnetic data presented herein were collected with the [100] direction of the crystal aligned with the external field. In the high-symmetry cubic limit, the principal axes of all four titanium(III) ions in the cell make an angle, θ, of 54.74° with the external magnetic field. Only in this orientation are all four ions in the unit cell magnetically equivalent. The 12 K cubic-to-orthorhombic phase transition of CsTiSH leads to a pronounced change in the magnetic properties of the $[Ti(OH_2)_6]^{3+}$ cation. Nevertheless, EPR data have shown that the g tensor remains axially symmetric and that the principal magnetic axes of the titanium(III) centers remain closely aligned along the directions corresponding to the 3-fold axes in the cubic phase.[13,29] Thus, with the [100] direction of the crystal aligned with the magnetic field, θ can be assumed to be ca. 55° at all temperatures.

Figure 4 displays magnetization data for Cs[Ga:Ti]SH with ca. 1% titanium(III) doping at fields ranging from 1 to 5.5 Tesla between 1.7 and 23.1 K. The magnetization of this sample shows a dramatic departure from Brillouin behavior with the data lying on one of several curves dictated by the strength of the magnetic field. No single curve may be adequately described by eq 6.

However, an excellent fit to the data obtained below ca. 6.5 K may be obtained using eq 5, considering terms up to third order in field, as shown in Figure 4, with $W^{(1)}$, $W^{(2)}$, and $W^{(3)}$ equal to $\pm 0.3572(4)$, $-0.01244(4)$ Tesla^{-1}, and $\mp 0.000326(5)$ Tesla^{-2}, respectively. This approach provides a more rigorous characterization of the electronic structure of the system compared to EPR and magnetic susceptibility studies, which yield thermally averaged values of the quantities $W^{(1)}$ and $W^{(1)2}/kT + W^{(2)}$, respectively. The errors quoted for the determined Zeeman coefficients are derived from a least-squares analysis of one data set and are representative of the precision of the fit. In total, three data sets were obtained, and the data were processed independently. Consistent results were obtained for the titanium(III) concentration, effective mass, and Zeeman coefficients. From a comparison of the three data sets, the Zeeman coefficients, with errors reflecting the accuracy, are estimated to be $W^{(1)} = \pm 0.357(5)$, $W^{(2)} = -0.0124(2)$ Tesla^{-1}, and $W^{(3)} = \mp 0.00032(5)$ Tesla^{-2}. At higher temperatures, the data deviate significantly from the fit, suggesting a population of higher-lying states whose energies have a very different dependence on external magnetic field. The large second-order contribution to the magnetization is unprecedented for a spin-half transition metal complex. It should be emphasized that this anomalous magnetic behavior was revealed by a comprehensive study at a range of fields and temperatures. High-field magnetization measurements are often used to determine the *g* value and spin multiplicity of the ground state of a paramagnet, and it is common practice to maintain a constant temperature and simply vary the field. This approach may well give rise to misleading results as it assumes from the outset that the magnetization conforms to a Brillouin function. To highlight this point, it is shown in Figure 4 that the data recorded at 2 K, at various field strengths, roughly straddle a Brillouin function (eq 6) with $W^{(1)} = \pm 0.460(2)$.

A previous EPR study of Cs[Ga:Ti]SH crystals revealed a range of chemically distinct $[Ti(OH_2)_6]^{3+}$ species at all concentrations of titanium(III), which differ in the magnitude of the distortion away from trigonal symmetry.[29] The degree of inhomogeneity was found to be small for a lightly doped sample (<0.5% titanium(III)), becoming more pronounced for 8.4%- and 31%-doped samples, and persisting up to 100% concentration.[29] Thus, the magnetic data for crystals highly doped with titanium(III) should strictly be analyzed in terms of a convolution of plots described by eq 5. However, this would be a gross over-parameterization of the data. We have found that at all concentrations, the magnetization data are very well described by eq 5, including terms to third-order only, with one unique value for the Zeeman coefficients. The question then is how meaningful are the Zeeman coefficients extracted from such an analysis? If one considers the mathematics of the problem, it is apparent that the second-order Zeeman coefficient, $W^{(2)}$, is the most reliable quantity derived, representing $W^{(2)}$ averaged over all ions in the sample. This is because the *i*th complex contributes a term, $BW_i^{(2)}$, to the overall magnetization, and the average over *N* complexes is $BW_N^{(2)}$. The fitting procedure does not yield accurate values for the average first- and third-order Zeeman coefficients as the average of a series of tan(*h*) functions cannot be described by a single tan(*h*) function. Our analysis suggests that the value of $W^{(1)}$, determined from a sample containing chemically distinct complexes with a range of $W^{(1)}$ values, slightly overestimates the true average value of $W^{(1)}$. We calculate that the values of $W^{(1)}$ obtained for the 13 and 51% could overestimate the average value by as much as 3%, depending on the degree of inhomogeneity. Though the error

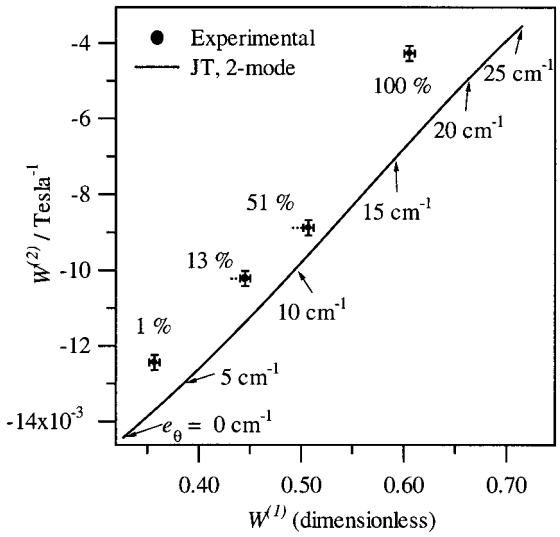

Figure 5. Experimental and theoretical values of $W^{(1)}$ and $W^{(2)}$ as a function of titanium(III) concentration and the strain parameter, e_θ, respectively. For each sample, the magnetization data were collected with the [100] direction of the single crystal aligned parallel with the external field. The theoretical plot, JT, was calculated using the same parameters as those employed to calculate the $W^{(1)}$ JT and $W^{(2)}$ JT relations in Figure 2.

is small, this is approximately 20 times the error obtained from a least-squares analysis of the data, and 3 times that estimated from repeated measurements. Figure 5 shows a plot of $W^{(2)}$ vs $W^{(1)}$ for all four crystals. For each sample, the ground-state Zeeman coefficients were obtained by modeling the data obtained between 1.7 and 6.5 K to eq 5. Consistent values for the Zeeman coefficients were obtained in this temperature range, suggesting that below 6.5 K, only the ground state is significantly populated, and that the factors that determine the values of the Zeeman coefficients such as strain vary little between 1.7 and 6.5 K. It is seen that the magnitudes of $W^{(1)}$ and $W^{(2)}$ increase and decrease sharply, respectively, with increasing titanium(III) concentration. The error bars on the values of $W^{(1)}$ and $W^{(2)}$ are those estimated from the repeated measurements of the 1%-doped sample. The dotted line to the left of the 13 and 51% titanium(III) sample points denotes the uncertainty in the value of $W^{(1)}$ owing to the uncertainty in the strain distribution. The greater the inhomogeneity, the lower the true average value of $W^{(1)}$.

4.2. Raman Data. Figure 6 shows Raman data from the 1%-titanium(III)-doped Cs[Ga:Ti]SH single crystal as a function of temperature. The spectra were recorded in $X'(Y'X')Y'$ scattering geometry, which permits the observation of Raman transitions of e_g symmetry only. The strong band centered at 52 cm^{-1} is also found in the pure CsGaSH salt and has been assigned as an external mode of sulfate coupled to the internal modes of the $[Ga(OH_2)_6]^{3+}$ complex.[29,36] In addition to the lattice band, a broad asymmetric band is found centered at 18 cm^{-1} and a very weak, very broad band is found in the energy range of 42−50 cm^{-1}. These bands are also found in the $X'(ZZ)Y'$ scattering geometry but are absent in the $X'(ZX')Y'$ experiment; they are not found in the Raman spectrum of CsGaSH and are consequently assigned as transitions due to the presence of the titanium(III) impurity. As the temperature is raised from 5 to 15 K, the band at 18 cm^{-1} broadens and loses intensity. At 25 K, the 18 cm^{-1} peak can barely be discerned from the baseline. The strong temperature dependence of this peak would not be

(36) Beattie, J. K.; Armstrong, R. S.; Best, S. P. *Spectrochim. Acta, Part A* **1996**, *51*, 539−548.

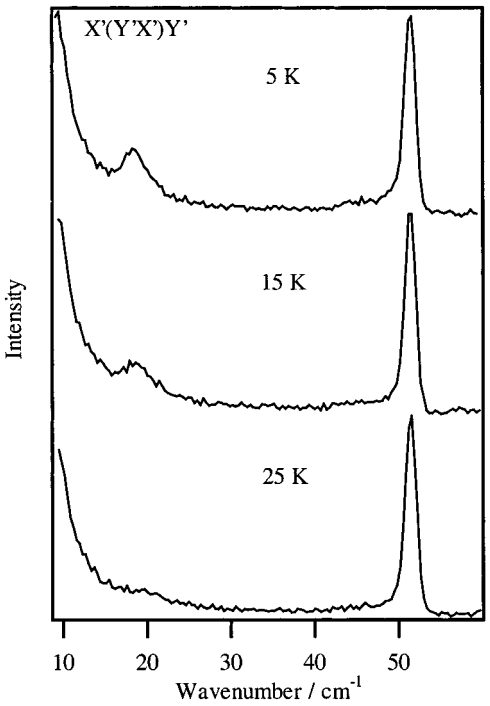

Figure 6. Single-crystal Raman spectra of Cs[Ga:Ti]SH (1% titanium(III)) as a function of temperature. Spectral bandwidth, 1.47 cm^{-1} at 20 cm^{-1}; integration time, 20 s; step size, 0.35 cm^{-1} at 20 cm^{-1}; radiation at sample, 80 mW, 514.5 nm.

expected for a vibrational Raman band but is typical for Raman transitions with electronic character.[37] Thus, this band is assigned as a vibronic Raman transition originating from the $[Ti(OH_2)_6]^{3+}$ impurity. The intensity of the band was not resonantly enhanced when the excitation wavelength was tuned towards the $^2T_{2g} \rightarrow {}^2E_g$ (O_h) electronic transition. The region of intensity between 42 and 50 cm^{-1} is of uncertain origin, being either electronic or vibrational in nature. The Raman spectra of the 13, 51, and 100% samples were also recorded in this energy region. The Raman spectrum of CsTiSH at 14.4 K exhibits a broad, weak band of E_g symmetry centered at ca. 17 cm^{-1}, which sharpens, gains intensity, and shifts two wavenumbers to higher energy as the sample is cooled through the phase transition to 1.9 K. A Raman band having a similar temperature dependence was also found in the isostructural rubidium alum, where it was assigned to a vibron, coupled strongly to the phase transition.[28] The Raman spectrum of CsTiSH and the rubidium analogue exhibit an unusually high background in the energy region of 10−300 cm^{-1} in $X'(Y'X')Y'$ and $X'(ZZ)Y'$ scattering geometries. The Raman bands of the 13%- and 51%-doped samples in this energy region are exceedingly broad and indistinct.

The spectra between 490 and 570 cm^{-1} in $X'(ZZ)Y'$ polarization displayed in Figure 7 contain the $\nu_1(TiO_6)$ and $\nu_1(GaO_6)$ modes, which correlate directly to the Ti−O and Ga−O bond lengths. Raman studies of the cesium alums have shown that the energy of the $\nu_1(M^{III}O_6)$ mode is roughly inversely proportional to the M^{III}−O bond length, with the $\nu_1(GaO_6)$ and $\nu_1(TiO_6)$ modes being located at 537 and 517 cm^{-1}, respectively.[38] Two bands of a_g symmetry are found in both the 13 and 51% titanium(III) samples at positions close to those expected for the $\nu_1(GaO_6)$ and $\nu_1(TiO_6)$ modes. The intensities

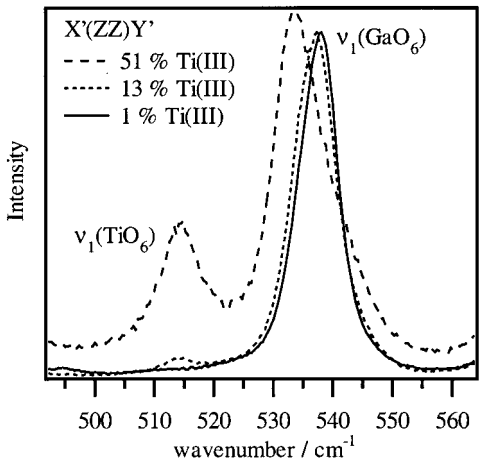

Figure 7. Single-crystal Raman spectra of Cs[Ga:Ti]SH for different concentrations of titanium(III), as indicated in the figure. This spectral region displays Raman bands assigned to the totally symmetric M^{III}−O stretch. Temperature at heat exchanger, 5 K; spectral bandwidth, 2.32 cm^{-1} at 530 cm^{-1}; integration time, 20 s; step size, 0.4 cm^{-1} at 530 cm^{-1}; radiation at sample, 80 mW, 514.5 nm.

of the bands, relative to that of the band due to $\nu_1(SO_4)$, change in accordance with the relative amounts of titanium(III) and gallium(III) in the sample, suggesting that the a_g components of $\nu_1(M^{III}O_6)$ are not strongly coupled and that the M^{III}−O bond lengths are broadly characteristic of the different metals in the pure alums. The $\nu_1(M^{III}O_6)$ modes broaden with increasing titanium(III) concentration, and their band shapes are clearly asymmetric in the 51% titanium(III) sample. The strong band assigned to $\nu_1(GaO_6)$ shifts to lower wavenumbers as the titanium(III) concentration increases, and the $\nu_1(TiO_6)$ band is centered at 514 cm^{-1} in both the 13 and 51% titanium(III) samples. The small shifts of the $\nu_1(TiO_6)$ and $\nu_1(GaO_6)$ modes from the values found in the CsTiSH and CsGaSH alums cannot be interpreted unambiguously; a discrepancy of similar magnitude was found for the $\nu_1(VO_6)$ mode in the isostructural CsVSH and RbVSH alums[38,39] despite the lack of a change in the V−O bond length.[24,40]

5. Discussion

5.1. Magnetization and Raman Data from 1%-Titanium(III)-Doped Cs[Ga:Ti]SH. We begin by discussing the data for the 1%-doped sample, where the degree of strain and inhomogeneity is minimal. The magnetization data provide a precise determination of the ground-state Zeeman coefficients to third-order. If the values of $W^{(1)}$ and $W^{(2)}$ are interpreted using a ligand-field Hamiltonian, where the vibrational coordinates are ignored, then from eqs 7 and 8 we obtain $k = 0.382$ and $\lambda = 25$ cm^{-1} ($\lambda_{free\ ion} = 153$ cm^{-1}), respectively.[41] These values are obviously not physical in view that the M^{III}−OH_2 bond is largely ionic[42] and λ is typically 120−130 cm^{-1} in titanium(III) complexes. Additionally, the experimental value of $W^{(3)}$ is almost a factor of 4 greater than that obtained using eq 9, and the model does not account for the vibronic Raman band found at 18 cm^{-1}. In Table 1 are listed the Zeeman coefficients, to

(37) Guha, S.; Chase, L. L. *Phys. Rev. B.* **1975**, *12*, 1658. Christie, J. H.; Lockwood, D. J. *Chem. Phys. Lett.* **1971**, *8*, 120.
(38) Best, S. P.; Beattie, J. K.; Armstrong, R. S. *J. Chem. Soc., Dalton Trans.* **1984**, 2611−2624.
(39) Tregenna-Piggott, P. L. W.; Best, S. P. *Inorg. Chem.* **1996**, *35*, 5730−5736.
(40) Beattie, J. K.; Best, S. P.; Del Favero, P.; Skelton, B. W.; Sobolev, A. N.; White, A. H. *J. Chem. Soc., Dalton Trans.* **1996**, 1481−1486.
(41) Note that the values of k and λ, so obtained by ligand-field theory, were incorrect in our initial communication of these data (ref 30).
(42) Best, S. P.; Figgis, B. N.; Forsyth, J. B.; Reynolds, P. A.; Tregenna-Piggott, P. L. W. *Inorg. Chem.* **1995**, *34*, 4605−4610.

Table 1. Zeeman Coefficients for the Low-Energy Vibronic Eigenstates of the Cs[Ga:Ti]SH System

$W^{(0)}$ (cm^{-1})	$W^{(1)}$ (dimensionless)	$W^{(2)}$ ($Tesla^{-1}$)	$W^{(3)}$ ($Tesla^{-2}$)
0[a]	±0.357(5)[a]	−0.0124(2)[a]	∓0.00032(5)[a]
0	±0.327	−0.0144	∓0.00030
16.4	±0.440	0.0123	∓0.00030
30.4	±0.368	−0.0185	∓0.00049
44.7	±0.470	0.0173	∓0.00049

[a] Experimental Zeeman coefficients for the ground state were determined by fitting eq 5 with $n = 3$ to the magnetization data presented in Figure 4. Theoretical Zeeman coefficients were calculated using parameters previously employed to fit the susceptibility data.[29] Eigenvalues were calculated for field strengths ranging from 0 to 5.5 Tesla, and the resulting relation fitted to a power series in field. In this field range, Zeeman coefficients higher than third-order are insignificant.

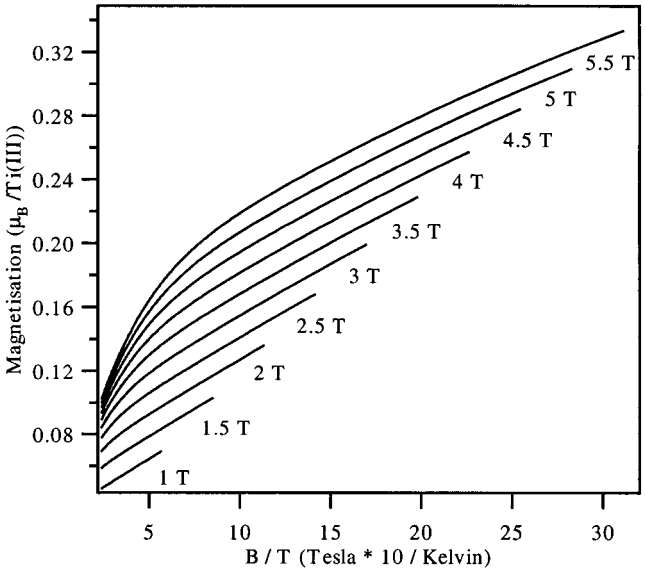

Figure 8. Magnetization vs *B*/*T*, calculated from the theoretical Zeeman coefficients presented in Table 1 for the same fields and temperatures used to determine the experimental magnetization data (Figure 4).

third-order, calculated using the two-mode model, for the four lowest-lying vibronic states. The magnetization vs *B*/*T* relation, calculated from the theoretical Zeeman coefficients, is presented in Figure 8, and corresponds closely to the experimental data set (Figure 4). In particular, the anomalously strong field dependence of the magnetization is reproduced, reflecting the good agreement between the calculated and experimental values of the ground-state value of $W^{(2)}$. The theoretical calculation also reproduces the dramatic change in the magnetic properties of the sample as the temperature is raised above ca. 6.5 K. This suggests that the Zeeman coefficients calculated for the first excitation also correspond closely to the experimental values. This gives us great confidence in assigning the vibronic Raman band at 18 cm^{-1} to the transition from the ground to the first excited state, depicted in Figure 3, the experimental energy being just 1.5 cm^{-1} greater than the calculated value. The second-order Zeeman coefficient of the first excited state has negative contributions from interaction with higher-lying states and a positive contribution from the ground state. The calculated value is large and positive: 0.0123 $Tesla^{-1}$. This means that the contribution from the first excited state to the overall value of $W^{(2)}$ in the ground state must be at least −0.0123 $Tesla^{-1}$. The calculated value is just a little higher, −0.0144 $Tesla^{-1}$, indicating that the giant ground-state second-order Zeeman effect is primarily a consequence of mixing with the first excited state

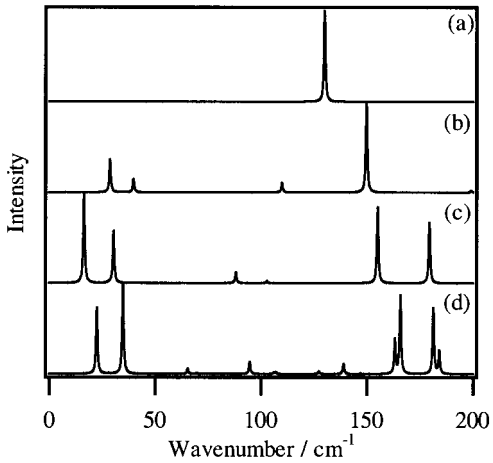

Figure 9. Theoretical vibronic Raman spectra as a function of the Jahn−Teller coupling strength and low-symmetry strain. All spectra were calculated with $\lambda = 130$ cm^{-1}, $\hbar\omega_1 = 894$ cm^{-1}, $\hbar\omega_2 = 53$ cm^{-1}, $T = 5$ K, and excitation wavelength = 514.5 nm; in all cases, a constant Lorentzian bandwidth is applied across the spectrum. The values for the Jahn−Teller coupling parameters, E_{JT1} and E_{JT2}, and the strain parameter, e_θ, are as follows: (a) E_{JT1}, E_{JT2}, and e_θ are set to zero; (b) $E_{JT1} = 90.1 \times 0.5$ cm^{-1}, $E_{JT2} = 53 \times 0.5$ cm^{-1}, $e_\theta = 0$; (c) $E_{JT1} = 90.1$ cm^{-1}, $E_{JT2} = 53$ cm^{-1}, $e_\theta = 0$; (d) $E_{JT1} = 90.1$ cm^{-1}, $E_{JT2} = 53$ cm^{-1}, $e_\theta = 20$ cm^{-1}.

through the magnetic field. This occurs both because of the close proximity of the ground and first excited states and because the first excited state resembles, electronically, the upper Kramers doublet, as discussed in section 2.2. The value of $W^{(2)}_{55°0,1}$ obtained from eq 14, assuming coupling to the low excitation only (E_{JT} = 53 cm^{-1} and $\hbar\omega$ = 53 cm^{-1}), is calculated to be −0.0106 $Tesla^{-1}$. Using the same parameters, the numerical value of $W^{(2)}$ is −0.0126 $Tesla^{-1}$ for the ground state and 0.0102 $Tesla^{-1}$ for the first excitation. The agreement is surprisingly good considering that eq 14 was formulated using perturbation theory, which is not strictly applicable for this set of parameters. As the temperature is raised above 6.5 K, the overall second-order contribution to the magnetization is strongly attenuated by the thermal population of the first excitation. It is apparent that the nature of the Jahn−Teller interaction is such that the observation of a giant second-order Zeeman effect is near optimal; if the Jahn−Teller coupling were much stronger, the first excitation would occur at lower energy and would be appreciably populated at low temperatures.

Calculations of the electronic Raman cross section are presented in Figure 9. The calculated spectrum in Figure 9a corresponds to that expected for zero Jahn−Teller coupling with λ set to 130 cm^{-1}. In this instance, one transition is expected between the Kramers doublets of the ^2E_g term. Spectrum c was calculated using the two-mode Jahn−Teller model, the parameters of which were given in section 3; half of the values of E_{JT1} and E_{JT2} were taken to calculate spectrum b. These calculations are very instructive as they illustrate the predicted changes in both the eigenvalues and the eigenvectors of the states resulting from Jahn−Teller coupling. It is seen that as the strength of Jahn−Teller coupling increases, the electronic Raman intensity is increasingly distributed across the vibronic spectrum. From the perspective of the ground state, the spin−orbit interaction is quenched as the electronic properties of the upper Kramers doublet are transferred to low-lying excitations. However, the electronic properties are not lost but redistributed, and the Raman intensity integrated over all states remains unchanged, as does the asymptotic value of the effective

magnetic moment. Thus, a rich electronic Raman spectrum is predicted for this system. It comes as a disappointment, therefore, that the transition between the ground and first excited state is the only electronic Raman transition that can be identified with certainty. We contend that the failure to observe additional electronic Raman bands is a consequence of lifetime broadening rather than a gross deficiency of the model. In cases where an electronic Raman band has been reported, further transitions at higher energy are often considerably broader[43] or are not observed at all.[44] Homogeneous broadening of the electronic Raman bands would also offer a plausible explanation for the anomalously high background found in the low-wavenumber spectrum of both CsTiSH and RbTiSH. Furthermore, EPR and Raman data presented previously provide evidence for coupling to additional modes, and indeed, the ^2E_g ground term must couple to all of the e_g phonon modes to a greater or lesser extent. Additional modes were not included in the original analysis of the paramagnetic susceptibility as this would have been an over-parameterization of the data; the magnetic properties of the ground state are dominated by the low-energy mode at 53 cm^{-1} on account of its low energy.[29] However, coupling to additional modes will contribute to the congestion in the electronic Raman spectrum. A more elaborate electronic Raman spectrum has recently been obtained for guanidinium vanadium sulfate, where an excellent reproduction of the electronic Raman profile was obtained using a formalism similar to that presented here.[44]

5.2. Magnetization Data from 13%-, 51%-, and 100%-Titanium(III)-Enriched Samples of Cs[Ga:Ti]SH and the Change in the Raman Spectrum as a Function of Strain. The magnetization data from crystals of Cs[Ga:Ti]SH with high titanium(III) concentrations yield, at best, bulk average values of $W^{(1)}$ and $W^{(2)}$ over all complexes in the sample, as discussed in the previous section. This is not the same as $W^{(1)}$ and $W^{(2)}$ for a single complex, subject to a given low-symmetry distortion, which are the quantities calculated. Nevertheless, our analysis of the data suggests that the degree of inhomogeneity is not so severe as to affect the analysis too adversely. In Figure 5, superimposed on the experimental plot of $W^{(2)}$ vs $W^{(1)}$ is the corresponding relation calculated using the two-mode model as a function of e_θ only. Although it should not be assumed that only the parameter e_θ varies as a function of titanium(III) concentration, $W^{(1)}$ and $W^{(2)}$ are extraordinarily sensitive to e_θ, and the theoretical plot is seen to give a good overall account of the experimental data. However, while the calculated plot gives a precise account of the $W^{(1)}$ vs $W^{(2)}$ relation, it is not accurate, and this must be attributed to a deficiency in the model. It should be emphasized, nonetheless, that the two-mode model gives by far the best account of the experimental data of the vibronic coupling models previously considered.[29]

Figure 9d shows the theoretical electronic Raman spectrum, calculated with e_θ set to 20 cm^{-1}; all other parameters are unchanged from their values used to calculate spectrum 9c. The low-symmetry distortion is predicted to give rise to a general shift of the vibronic excitations to higher energy, a redistribution of the electronic Raman intensity, and a splitting of some of the degenerate states. Thus, the electronic Raman bands arising from a sample with a distribution of species subject to varying amounts of low-symmetry strain are predicted to be broad and asymmetric. Strain broadening undoubtedly makes an important contribution to the band shapes of the electronic Raman transitions observed at low temperatures, and this is emphasized in Figure 3. The predicted change in the energy of the first excitation with increasing strain is borne out by the Raman data of CsTiSH. However, the interpretation of the temperature dependence of the Raman spectrum of salts, which exhibit a vibronically induced structural instability, is a seemingly complicated affair, requiring a detailed treatment of the cooperative Jahn−Teller interaction.[34] Instead, we avail ourselves of the opportunity to interpret Raman data previously reported for titanium(III) lightly doped into the isostructural CsAlSH alum.[45] A broad band of e_g activity was found centered at an energy of 21.3 cm^{-1}, increasing quadratically with stress applied along the [100] direction of the crystal. Though the data were inconsistent with the model fashionable at the time,[21] they are wholly consistent with our two-mode model. Figure 10 shows the variation of the low-lying excitations as a function of e_θ. It is shown that for small values of e_θ, the variation of the low-energy excitation with e_θ can be described as quadratic.

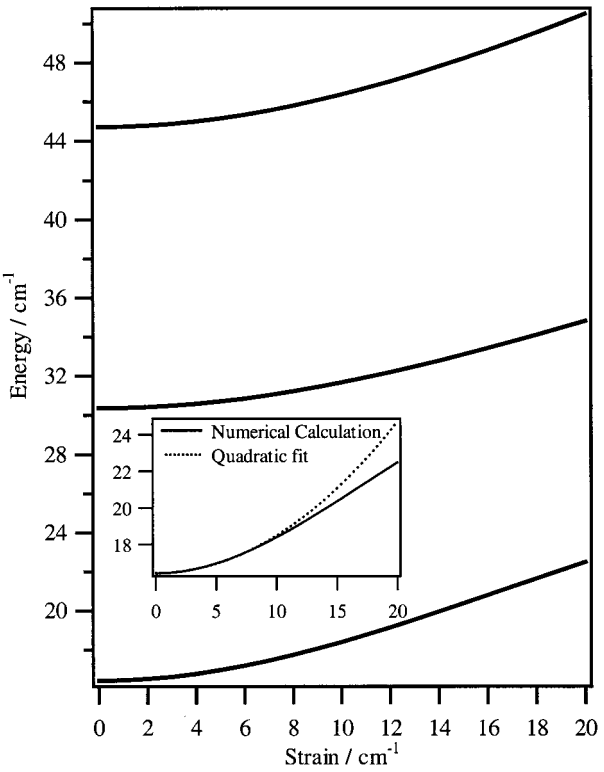

Figure 10. Energies of the first three vibronic excitations relative to the ground state as a function of the strain parameter, e_θ, calculated using the two-mode Jahn−Teller model, the parameters of which are given in the caption of Figure 2. The inset shows a fit to the energy of the first excitation at e_θ values between 0 and 8 cm^{-1}, assuming a quadratic dependence of the energy on e_θ.

6. Conclusion

In this work, the strong influence that Jahn−Teller coupling can have on the magnetic properties of octahedrally coordinated transition metals with orbital triplet ground terms has been demonstrated by a magnetization and Raman study of the $Cs[Ga:Ti](SO_4)_2 \cdot 12H_2O$ system. The anomalous magnetic prop-

(43) Gächter, B. F.; Konigstein, J. A. *Solid State Commun.*, **1974**, *14*, 361.
(44) Spichiger, D.; Carver, G.; Dobe, C.; Bendix, J.; Tregenna-Piggott, P. L. W.; Meier, R.; Zahn, G. *Chem. Phys. Lett.* **2001**, *337*, 391.
(45) Chase, L. L.; Glynn, T. J.; Hayes, W.; Rushworth, A. J.; Ryan, J. F.; Walsh, D.; De Goer, A. M. *Proceedings of the Fifth International Conference on Raman Spectroscopy, Freiburg, Germany, 1976*; Schmid, E. D., Brandmueller, J., Kiefer, W., Eds.; Hans Ferdinand Schulz Press: 1976; pp 660−661.

erties are a result of a delicate balance between the spin−orbit and Jahn−Teller interactions. Indeed, it is not an easy task to find an alternative set of parameters, which would predict more intriguing magnetic behavior. As predicted by Ham[35] "...as a consequence of the Jahn−Teller interaction...all types of perturbing operators...should give rise to enhanced second-order effects in the ground state, due to interaction with excited vibronic states." We believe this to be one of the most beautiful and illustrative examples of this behavior.

We must own that such anomalous magnetic properties will occur only when certain requirements are fulfilled. From the pronounced dependence of the Zeeman coefficients on the titanium(III) concentration, it can be concluded that the anomalous magnetic behavior, manifested by the dynamical Jahn−Teller effect, is strongly attenuated by low-symmetry distortions. It is expected, therefore, that the magnetic properties of low-symmetry transition metal complexes, with orbital triplet ground terms, should be well described using methods developed by the votaries of ligand-field[46] and density functional[47] theory. In addition to the requirement of high symmetry, orbitals on the ligands should be available for π-bonding and the metal−ligand π-interaction should be highly anisotropic, as is the case for the water ligand.[42] Only in this instance will the energies of the t_{2g} orbitals exhibit sufficient sensitivity to a given vibration of the complex. Finally, the strength of the vibronic interaction generally increases as a function of $E_{JT}/\hbar\omega$, and thus the most spectacular effects are expected when the electronic states are involved in moderate coupling with a low-energy vibration. Great attention should be paid to magnetic data from high-symmetry complexes formed with ligands such as water, hydroxide, imidazole, pyridine, imidazolate, thiophene, amides, carboxylates, oxalate, actylacetonate, and porphyrins, where significant Jahn−Teller coupling involving the librational modes of these ligands can be expected.

Acknowledgment. This work is dedicated to the late Mary O'Brien, who was involved in the earlier stages of the project. Stimulating discussions with Jesper Bendix, Stephen Best, Arnout Ceulemans, and Høgni Weihe are also acknowledged. Financial assistance from the Swiss National Science Foundation is greatly appreciated.

IC010277F

(46) Ballhausen, C. J. *Introduction to Ligand Field Theory*; McGraw-Hill: New York, 1962. Schäffer, C. E. *Struct. Bonding (Berlin)*, **1968**, *5*, 68−95. Gerloch, M. *Magnetism and Ligand-Field Analysis*; Cambridge University Press: New York, 1983.

(47) Deeth, R. J. *Struct. Bonding (Berlin)* **1995**, *82*, 1−42. Chermette, H. *Coord. Chem. Rev.* **1998**, *180*, 699−721.